Transitions between phases with equal wavenumbers in a double Ising spin model. Application to betaine calcium chloride dihydrate

1998 J. Phys.: Condens. Matter 10 6883

(http://iopscience.iop.org/0953-8984/10/31/007)

J. Phys.: Condens. Matter **10** (1998) 6883–6896. Printed in the UK PII: S0953-8984(98)92574-7

Transitions between phases with equal wavenumbers in a double Ising spin model. Application to betaine calcium chloride dihydrate

Boris Neubert†§, Michel Pleimling‡‖ and Rolf Siems†

† Theoretische Physik, Universität des Saarlandes, Postfach 151150, D-66041 Saarbrücken, Germany

‡ Institut für Theoretische Physik, Technische Hochschule, D-52056 Aachen, Germany

Received 17 March 1998

Abstract. A double Ising spin model for uniaxially structurally modulated materials exhibits as a special feature phase transitions between phases with equal wavenumbers but different pseudo-spin configurations. The character of these 'internal' transitions is investigated in the mean-field approximation, with the mean-field transfer-matrix method, and in Monte Carlo simulations. The structural changes at the transitions are characterized by different strengths of harmonics in a Fourier analysis of the spatial modulation. A dielectric anomaly in the phase diagram of betaine calcium chloride dihydrate (BCCD) and seemingly contradictory structure analyses are explained.

1. Introduction

Materials exhibiting commensurately and incommensurately structurally modulated phases have been extensively investigated during recent years. BCCD, $(CH_3)_3NCH_2COO \cdot CaCl_2 \cdot H_2O$, is an outstanding example: it shows a rich variety of phases, and exhibits many intricate phenomena in its phase diagram, such as indications for accumulation points of structure branchings, and the so-called dielectric T_S-anomaly [1]. The problem of the modulation and its temperature dependence still poses many open questions. The plenitude of experimental results has led to a continuing theoretical interest, and many different models for their explanation have been developed (for reviews see references [2, 3]).

We recently used the concept of symmetry-adapted local modes [4] to derive the double Ising spin (DIS) model [5, 6] as a symmetry-based pseudo-spin model with two two-component pseudo-spin variables per crystallographic unit cell: the symmetry-breaking atomic displacements occurring at the transition from the high-temperature (high-symmetry) para-phase to the modulated phases at lower temperatures are expanded in terms of an appropriately chosen basis set, and the pseudo-spin components τ and σ are the signs of the relevant coordinates [7, 8]. In the case of materials with the high-temperature-phase space group *Pnma* (e.g. BCCD), this approach yields the Hamiltonian of the DIS model [5]:

§ Present address: Departamento de Física de la Materia Condensada, Facultad de Ciencias, Universidad del País Vasco, Apartado 644, Bilbao, Spain; e-mail: neubert@lusi.uni-sb.de.

‖ E-mail: pleim@physik.rwth-aachen.de.

0953-8984/98/316883+14$19.50

$$H = K\sum_{ijk}\tau_{ijk}\tau_{ij(k+1)} + L\sum_{ijk}\sigma_{ijk}\sigma_{ij(k+1)} + \frac{M}{2}\sum_{ijk}(\sigma_{ijk}\tau_{ij(k+1)} - \tau_{ijk}\sigma_{ij(k+1)}) + J\sum_{ijk}\tau_{ijk}(\tau_{(i+1)jk} + \tau_{i(j+1)k}) + J'\sum_{ijk}\sigma_{ijk}(\sigma_{(i+1)jk} + \sigma_{i(j+1)k}). \quad (1)$$

i, j, k label the pseudo-spin positions along the $\boldsymbol{a}$-, $\boldsymbol{b}$-, $\boldsymbol{c}$-directions respectively. At $T = 0$, the in-layer couplings $J < 0$, $J' < 0$ lead to a ferro-ordering of the layers perpendicular to $\boldsymbol{c}$. In the $\boldsymbol{c}$-direction, frustrations and therefore modulations arise because of the antagonistic effects of the symmetric nearest-neighbour interactions K and L on the one hand and the antisymmetric interaction $M > 0$ on the other hand. The stable structures (pseudo-spin profiles) obtained from the statistical mechanics treatment of H are characterized by their wavenumbers q given in units of 2π/(pseudo-spin spacing).

At $T = 0$, five stable phases are separated by multiphase lines in the K/M–L/M plane. Along these lines, an infinity of different phases are degenerate. We restrict ourselves to ferroelectric τ–τ interactions, i.e. $K < 0$; the phase diagram for $K > 0$ is obtained by exploiting the properties of H. In the following, we will consider the multiphase lines (a) and (b) separating, in the notation of reference [6], phase V (the pseudo-spin structure repeats itself after four layers) from the ferroelectric phase I (all τ- and σ-spins in ferro-order) and the mixed phase III (τ-spins in ferro-, σ-spins in antiferro-order along $\boldsymbol{c}$) respectively.

For low temperatures, all phases degenerate at line (a) (with $K < 0$ and $L < 0$) and obeying certain rules have a finite stability range in the vicinity of this line [6]. Incidentally, this also holds for the four-state chiral clock model which can be derived from the DIS model for the case where $K = L < 0$ and $J = J' < 0$ [9].

In contrast to this, in the vicinity of line (b) (with $K < 0$ and $L > 0$) only four different phases (characterized by the wavenumbers $q = 0$, $\frac{1}{8}$, $\frac{1}{6}$, and $\frac{1}{4}$) are stable at very low temperatures [6]. Other phases are created at higher temperatures by structure combination branching processes.

In the present paper, we report on a remarkable type of transition in the DIS model for the case where $K < 0$ and $L > 0$: these 'internal' transitions occurring at certain temperatures T_{int} are characterized by a structural change in the pseudo-spin arrangement which is not accompanied by a change of q and—in some cases—not even by a change of the symmetries of the profile.

The paper is organized as follows. In section 2, the pseudo-spin profiles calculated in the mean-field approximation (MFA) are discussed. The results are substantiated in section 3 by employing the mean-field transfer-matrix method and Monte Carlo simulations, which prove that these transitions are not artefacts of the MFA. In section 4, the internal transition in the $q = \frac{1}{8}$ phase of the DIS model is used to explain a dielectric anomaly in the fourfold phase of BCCD as well as seemingly contradictory experimental structure analysis results. Section 5 contains a summarizing discussion.

2. Mean-field investigation of the internal transitions

The mean-field approximation is often used for analysing the finite-temperature behaviour of pseudo-spin models. The starting point is the variational Hamiltonian

$$H_0 = -\sum_{ijk}\boldsymbol{\eta}_k \cdot \boldsymbol{S}_{ijk} \quad (2)$$

for systems with a modulation in the (001) direction, with $\boldsymbol{S}_{ijk} = (\tau_{ijk}, \sigma_{ijk})$. The product $\boldsymbol{\eta}_k \cdot \boldsymbol{S}_{ijk}$ describes the interaction of the spin $\boldsymbol{S}_{ijk}$ (which in our case has two components)

with a site-dependent mean-field η_k depending on the averages of the neighbouring spins. The mean values $t_\ell = \langle \tau_{ij\ell} \rangle$ and $s_\ell = \langle \sigma_{ij\ell} \rangle$ of the pseudo-spins τ and σ in the layer ℓ are determined by the MFA equilibrium equations ($\beta = 1/k_B T$):

$$\begin{aligned} t_\ell &= \tanh(\beta \eta_{1,\ell}) \\ s_\ell &= \tanh(\beta \eta_{2,\ell}) \end{aligned} \tag{3}$$

with the mean fields

$$\begin{aligned} \eta_{1,\ell} &= -4Jt_\ell - K(t_{\ell+1} + t_{\ell-1}) + \frac{M}{2}(s_{\ell+1} - s_{\ell-1}) \\ \eta_{2,\ell} &= -4J's_\ell - L(s_{\ell+1} + s_{\ell-1}) - \frac{M}{2}(t_{\ell+1} - t_{\ell-1}). \end{aligned}$$

Figure 1 shows a typical mean-field phase diagram in the plane $\lambda = 0.1$, $j = j' = -0.25$, where we have introduced the reduced interaction parameters $\kappa = K/M, \lambda = L/M, j = J/M, j' = J'/M$ and $\kappa_- = \frac{1}{2}(\kappa - \lambda)$; $\theta = k_B T/M$ denotes the reduced temperature. The shaded areas contain incommensurate and higher-order commensurate phases. The different commensurate phases are characterized by their wavenumbers. Para-phase, ferro-phase, and modulated phases meet at the Lifshitz point (LP). At $\theta = 0$ the cut through the temperature–interaction phase diagram considered intersects the multiphase line at the multiphase point MP.

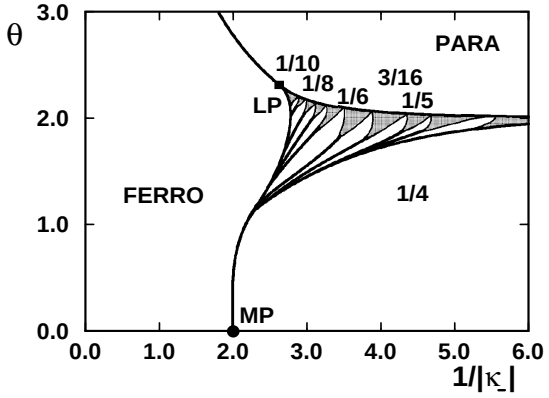

Figure 1. The reduced-temperature–interaction phase diagram of the DIS model with $\lambda = 0.1$ and $j = j' = -0.25$ (see the text). Shown are the paraelectric, the ferroelectric, and a few commensurate phases. Higher-order commensurate and incommensurate phases are contained in the hatched areas. LP is the Lifshitz point, MP the multiphase point. θ is the reduced temperature $k_B T/M$, whereas κ_- is given by $\kappa_- = \frac{1}{2}(\kappa - \lambda)$. The phases are characterized by quotients $q = m/n$ giving the modulation wavenumbers in units of $2\pi/$(pseudo-spin spacing).

The existence of accumulation points of structure branchings in the case where $K < 0$ and $L > 0$ was verified [5] by formulating the mean-field equilibrium equations (3) as a four-dimensional mapping and using a fixed-point technique analogous to that employed for the ANNNI model [10]. Also calculated were the self-energies and the interaction of the discommensurations.

As a consequence of the signs of the parameters K, L, and M (i.e. $K < 0$, $L > 0$, and $M > 0$), all phases degenerate at the multiphase line (b) consist of bands of two types of two-layer sequence, namely $\left(\begin{smallmatrix} + & + \\ - & + \end{smallmatrix}\right)$ and $\left(\begin{smallmatrix} - & - \\ + & - \end{smallmatrix}\right)$, where the upper (lower) symbols represent the signs of the τ-spin (σ-spin). We introduce a bracketed notation $\langle A_1 \cdots A_k \rangle$ for the

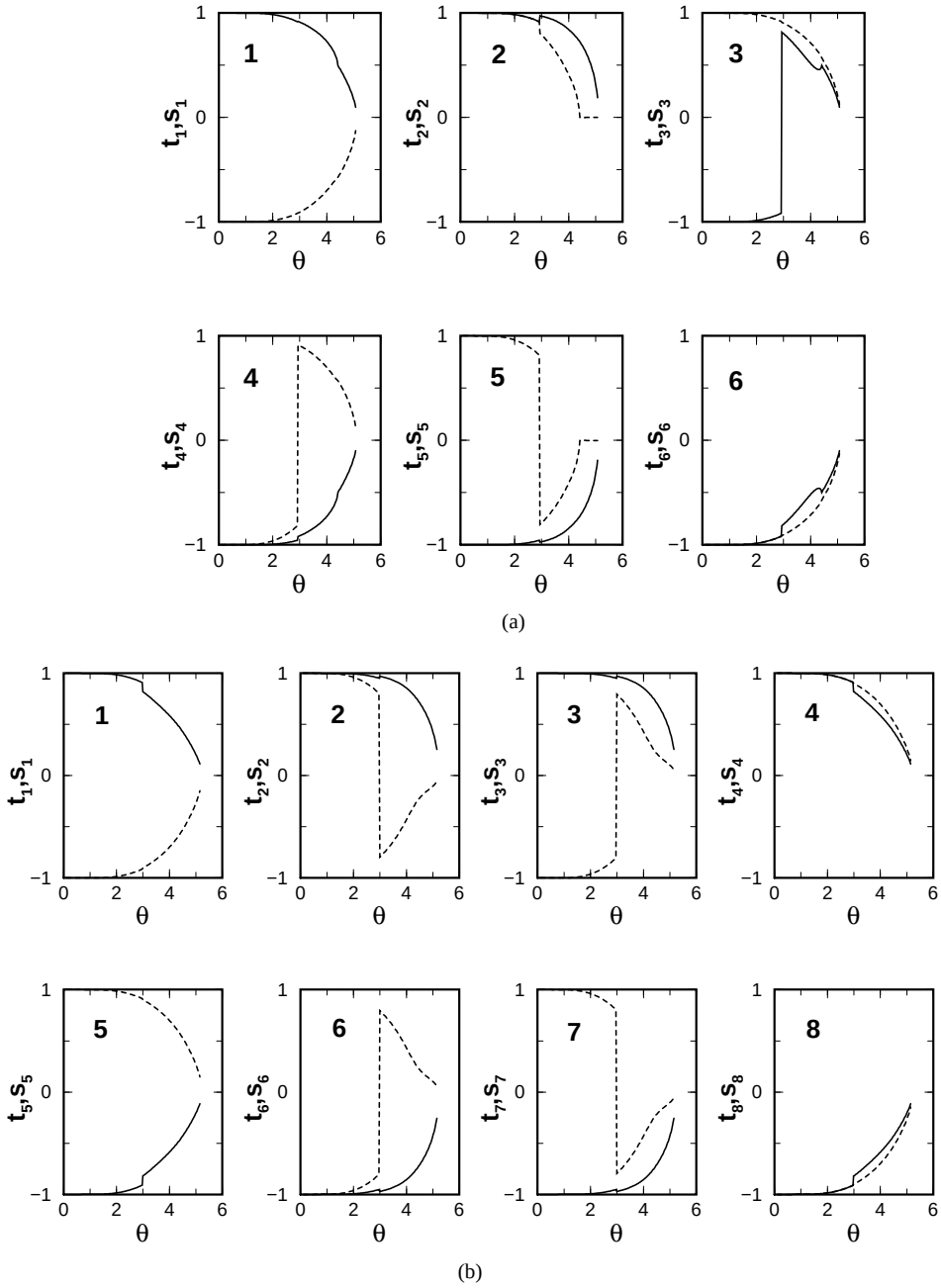

Figure 2. Pseudo-spin profiles for (a) the ⟨12⟩ phase ($q = \frac{1}{6}$) and (b) the ⟨2⟩ phase ($q = \frac{1}{8}$) as functions of the reduced temperature θ with $\lambda = 0.05$ and $j = j' = -1$. Shown are the mean values t_ℓ (solid lines) and s_ℓ (dashed lines), for layers ℓ from 1 to the modulation length, i.e. from 1 to 6 for case (a) and from 1 to 8 for case (b).

different phases: for example, ⟨23⟩ denotes a repetitive pseudo-spin structure consisting of a band with two $\left(\begin{smallmatrix}+ & +\\ - & +\end{smallmatrix}\right)$ sequences followed by a band with three $\left(\begin{smallmatrix}- & -\\ + & -\end{smallmatrix}\right)$ sequences. The

wavenumber for the above phase is

$$q = k \Big/ \left(4 \sum_{i=1}^{k} A_i \right).$$

The equilibrium pseudo-spin profiles for configurations with a fixed wavenumber q at a given temperature are obtained by finding the self-consistent solutions of the equations (3). This is done by starting from different initial spin configurations with the same modulation period and iterating. The respective free energies are calculated and the solution with the lowest free energy describes the stable spin configuration. Keeping λ, j, and j' fixed, the reduced parameters θ and κ_- are then varied in such a way that the resulting line $\theta(\kappa_-)$ always lies wholly in the stability region of the phase under investigation. Figure 2 shows the spin profiles obtained for the phases $\langle 12 \rangle$ (wavenumber $q = \frac{1}{6}$) and $\langle 2 \rangle$ ($q = \frac{1}{8}$) with $\lambda = 0.05$ and $j = j' = -1$. For both wavenumbers there is a discontinuous internal phase transition. At higher temperatures, the $q = \frac{1}{6}$ phase also exhibits a continuous transition to a modification with two disordered layers.

The spin profiles obtained for the $\langle 2 \rangle$ phase (for layers 1 to 8, i.e. for one modulation period) exhibit symmetries given by

(a) at low temperatures:

t:	t_1	t_2	t_2	t_1	$-t_1$	$-t_2$	$-t_2$	$-t_1$
s:	$-s_1$	s_2	$-s_2$	s_1	s_1	$-s_2$	s_2	$-s_1$

(b) at high temperatures:

t:	t_1	t_2	t_2	t_1	$-t_1$	$-t_2$	$-t_2$	$-t_1$
s:	$-s_1$	$-s_2$	s_2	s_1	s_1	s_2	$-s_2$	$-s_1$.

At a reduced temperature θ_{int}, the σ-spin averages change signs in layers 2, 3, 6, and 7, whereas the symmetry elements of the spin profiles are left unchanged. Furthermore, the τ-spins (in all layers) also show discontinuities at θ_{int}.

For the $\langle 12 \rangle$ phase, the spin profiles in the vicinity of the discontinuous transition are:

(a) at low temperatures:

t:	t_1	t_1	$-t_2$	$-t_3$	$-t_3$	$-t_2$
s:	$-s_1$	s_1	s_2	$-s_3$	s_3	$-s_2$

(b) at high temperatures:

t:	t_1	t_2	t_3	$-t_1$	$-t_2$	$-t_3$
s:	$-s_1$	s_2	s_3	s_1	$-s_2$	$-s_3$.

In this case the τ-spins in layer 3 (and the σ-spins in layers 4 and 5) change signs, leading to a change of the symmetries of the profile.

In general, not all combinations of the signs of the spins were taken as possible starting points for solving the equilibrium equations self-consistently. However, we substantiated our results for selected values of the parameters by considering all 2^{11} (phase $\langle 12 \rangle$) or 2^{15} (phase $\langle 2 \rangle$) possible sign combinations (changing the signs of all spins leaves the free energy unchanged).

In order to characterize the different modifications, a Fourier analysis of the spatial modulation of t_ℓ and s_ℓ was performed. In the following, the results for the $q = \frac{1}{8}$ phase are discussed, as they will be needed for the application to BCCD in section 4. For reduced temperatures slightly below ($\theta = 2.967$) and above ($\theta = 2.993$) the reduced temperature θ_{int} of the internal transition, the pseudo-spin averages (profiles) for one period of the spatial

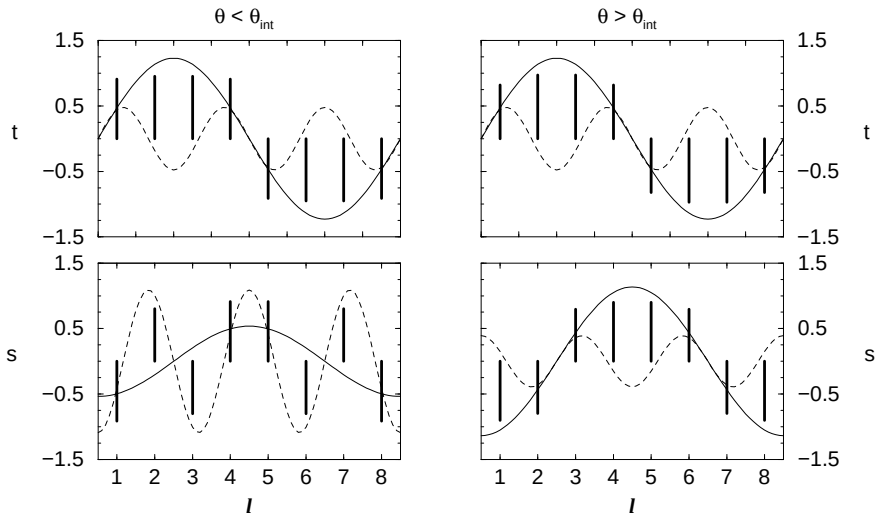

Figure 3. The pseudo-spin profiles t_ℓ (upper part) and s_ℓ (lower part) of the $q = \frac{1}{8}$ phase for reduced temperatures slightly below ($\theta = k_B T/M = 2.967$, left-hand side) and slightly above ($\theta = 2.993$, right-hand side) the internal transition $\theta_{\rm int}$. Only first-order (solid lines) and third-order (dashed lines) harmonics in sines (cosines) are present in the Fourier expansion of t_ℓ (s_ℓ).

modulation are shown in figure 3 together with their harmonics. Due to the symmetries in the pseudo-spin profiles, the Fourier components of t_ℓ (s_ℓ) are all odd (even) about $\ell = \frac{1}{2}$, and only odd orders in sines (cosines) occur in the Fourier series:

$$t_\ell = a_1 \sin\left(\frac{\pi}{4}\left[\ell - \frac{1}{2}\right]\right) + a_3 \sin\left(\frac{3\pi}{4}\left[\ell - \frac{1}{2}\right]\right) \tag{4}$$

$$s_\ell = b_1 \cos\left(\frac{\pi}{4}\left[\ell - \frac{1}{2}\right]\right) + b_3 \cos\left(\frac{3\pi}{4}\left[\ell - \frac{1}{2}\right]\right). \tag{5}$$

Upon cooling (see figure 4), the relative strength of the third-order harmonic with respect to the first-order harmonic increases smoothly from zero near the transition to the para-phase to about a third near $\theta_{\rm int}$ (both for the t- and s-profiles). When dropping below $\theta_{\rm int}$, only a slight increase in a_1 and a_3 but remarkable changes in b_1 and b_3 occur: b_3 jumps from 0.391 at $\theta = 2.993$ to -1.089 at $\theta = 2.967$ while $|b_1|$ decreases from 1.136 to 0.536. Below $\theta_{\rm int}$, the s-profile is governed by the strong third-order harmonic ($|b_3/b_1| > 2.03$), which continuously increases to the ground-state value $|b_3| = 1.307$, whereas the first harmonic keeps its nearly constant value $|b_1| = 0.54$.

In the MFA, these discontinuous internal phase transitions were obtained for all phases investigated for the DIS model, excepting only the $\langle 1 \rangle$ and the $\langle \infty \rangle$ (ferro-) phases. They occur for all values of λ and κ as long as $\lambda > 0$ and $\kappa < 0$, as well as for all in-layer couplings j and j' (even for very large values).

3. Verification by mean-field transfer-matrix and Monte Carlo methods

In the previous section, the DIS model was treated in the mean-field approximation. The question arises of whether the observed internal transitions are an artefact of this approximation or whether they are also present if one goes beyond mean-field theory.

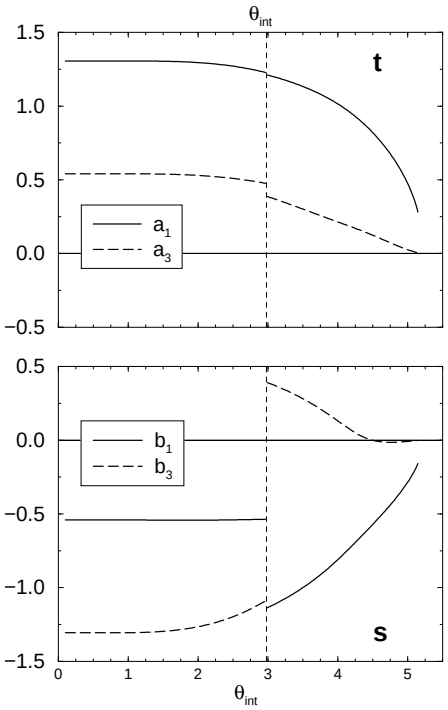

Figure 4. The amplitudes of the first- and third-order harmonics in the pseudo-spin profiles t_ℓ and s_ℓ of the $q = \frac{1}{8}$ phase as functions of the reduced temperature $\theta = k_B T/M$ (see equations (4) and (5)). The internal phase transition at θ_{int} separates the low-temperature modification with the dominant third harmonic in s from the much less anharmonic high-temperature modification.

This problem should indeed be considered: in the MFA, the axial next-nearest-neighbour Ising (ANNNI) model [11] with weak in-layer couplings exhibits, for example, phase transitions from the low-temperature phases to high-temperature asymmetric and partially disordered phases [12]. Nakanishi [13] was able to show that these phases are MFA artefacts by demonstrating that they do not occur if the mean-field transfer-matrix (MFTM) method is used, in which the interactions in the direction of the modulations are treated exactly. The same conclusion was drawn from Monte Carlo simulations [14].

In the MFTM method, the variational Hamiltonian for the DIS model is

$$H_0 = K \sum_{ijk} \tau_{ijk}\tau_{ij(k+1)} + L \sum_{ijk} \sigma_{ijk}\sigma_{ij(k+1)} + \frac{M}{2} \sum_{ijk} (\sigma_{ijk}\tau_{ij(k+1)} - \sigma_{ij(k+1)}\tau_{ijk}) - \sum_{ijk} \boldsymbol{\eta}_k \cdot \boldsymbol{S}_{ijk}. \tag{6}$$

In the MFA variational Hamiltonian (2), all interactions are described in terms of mean fields. In contrast, in equation (6), site-dependent mean fields are only introduced for the interactions perpendicular to the direction of modulation. As the two-component mean fields $\boldsymbol{\eta}_k$ do not depend on the indices i and j, the problem is reduced to one dimension and the indices i and j will be omitted.

Using the Bogoliubov variational principle, the MFTM free energy is given by

$$F = 2J \sum_\ell t_\ell^2 + 2J' \sum_\ell s_\ell^2 + \sum_\ell \eta_{1,\ell} t_\ell + \sum_\ell \eta_{2,\ell} s_\ell - k_B T \ln Z \tag{7}$$

with

$$Z = \mathrm{Tr}\exp\Bigg(\tilde{K}\sum_{\ell}\tau_\ell\tau_{\ell+1} + \tilde{L}\sum_{\ell}\sigma_\ell\sigma_{\ell+1} + \frac{\tilde{M}}{2}\sum_{\ell}(\tau_{\ell+1}\sigma_\ell - \sigma_{\ell+1}\tau_\ell) + \sum_{\ell}(h_{1,\ell}\tau_\ell + h_{2,\ell}\sigma_\ell)\Bigg) \tag{8}$$

and $\tilde{K} = \beta K$, $\tilde{L} = \beta L$, $\tilde{M} = \beta M$, and $h_{1,\ell} = \beta\eta_{1,\ell}$, $h_{2,\ell} = \beta\eta_{2,\ell}$. In order to calculate the partition function Z we introduce the transfer matrix

$$\mathbf{T}_\ell = \begin{pmatrix} \mathrm{e}^{h_{1,\ell}+h_{2,\ell}} & 0 & 0 & 0 \\ 0 & \mathrm{e}^{h_{1,\ell}-h_{2,\ell}} & 0 & 0 \\ 0 & 0 & \mathrm{e}^{-h_{1,\ell}+h_{2,\ell}} & 0 \\ 0 & 0 & 0 & \mathrm{e}^{-h_{1,\ell}-h_{2,\ell}} \end{pmatrix} \times \begin{pmatrix} \mathrm{e}^{\tilde{K}+\tilde{L}} & \mathrm{e}^{\tilde{K}-\tilde{L}+\tilde{M}} & \mathrm{e}^{-\tilde{K}+\tilde{L}-\tilde{M}} & \mathrm{e}^{-\tilde{K}-\tilde{L}} \\ \mathrm{e}^{\tilde{K}-\tilde{L}-\tilde{M}} & \mathrm{e}^{\tilde{K}+\tilde{L}} & \mathrm{e}^{-\tilde{K}-\tilde{L}} & \mathrm{e}^{-\tilde{K}+\tilde{L}+\tilde{M}} \\ \mathrm{e}^{-\tilde{K}+\tilde{L}+\tilde{M}} & \mathrm{e}^{-\tilde{K}-\tilde{L}} & \mathrm{e}^{\tilde{K}+\tilde{L}} & \mathrm{e}^{\tilde{K}-\tilde{L}-\tilde{M}} \\ \mathrm{e}^{-\tilde{K}-\tilde{L}} & \mathrm{e}^{-\tilde{K}+\tilde{L}-\tilde{M}} & \mathrm{e}^{\tilde{K}-\tilde{L}+\tilde{M}} & \mathrm{e}^{\tilde{K}+\tilde{L}} \end{pmatrix}.$$

For a commensurate phase with period p, the mean fields repeat themselves after p layers. The partition function (8) is then given by $Z = \alpha_{\max}^{N/p}$ where $\alpha_{\max}$ is the maximum eigenvalue of the matrix product $\prod_{\ell=1}^{p}\mathbf{T}_\ell$, and N is the number of layers in the crystal.

The mean values t_ℓ and s_ℓ are calculated from

$$t_\ell = \frac{\partial \ln\alpha_{\max}}{\partial h_\ell^1} = \frac{1}{\alpha_{\max}}\langle\alpha_{\max}\left|\mathbf{T}_1\cdots\mathbf{T}_{\ell-1}\mu^t\mathbf{T}_\ell\cdots\mathbf{T}_p\right|\alpha_{\max}\rangle$$
$$s_\ell = \frac{\partial \ln\alpha_{\max}}{\partial h_\ell^2} = \frac{1}{\alpha_{\max}}\langle\alpha_{\max}\left|\mathbf{T}_1\cdots\mathbf{T}_{\ell-1}\mu^s\mathbf{T}_\ell\cdots\mathbf{T}_p\right|\alpha_{\max}\rangle. \tag{9}$$

$\langle\alpha_{\max}|$ and $|\alpha_{\max}\rangle$ are the left and the right eigenvectors corresponding to the eigenvalue $\alpha_{\max}$, whereas the matrices $\boldsymbol{\mu}^t$ and $\boldsymbol{\mu}^s$ are given by

$$\boldsymbol{\mu}^t = \begin{pmatrix} 1 & 0 & 0 & 0 \\ 0 & 1 & 0 & 0 \\ 0 & 0 & -1 & 0 \\ 0 & 0 & 0 & -1 \end{pmatrix} \qquad \boldsymbol{\mu}^s = \begin{pmatrix} 1 & 0 & 0 & 0 \\ 0 & -1 & 0 & 0 \\ 0 & 0 & 1 & 0 \\ 0 & 0 & 0 & -1 \end{pmatrix}.$$

The mean fields

$$\eta_{1,\ell} = -4Jt_\ell \qquad \eta_{2,\ell} = -4J's_\ell \tag{10}$$

result from the minimization of the free energy (7). Equations (9) and (10) are to be solved self-consistently.

As an example, we will discuss the application of this method to the $q = \frac{1}{8}$ phase. Calculations within the mean-field approximation (see the previous section) yield a first-order phase transition at θ_{int} between a low- and a high-temperature modification (figure 2). These two spin profiles are used as starting points for the self-consistent solution of the MFTM equations (9) and (10).

Figure 5 shows the resulting free energies obtained by varying the model parameters in the same manner as in the previous section, i.e. one proceeds along the same $\theta(\kappa_-)$ curve as for the MFA calculations. It is clearly seen that the free-energy curves of the two modifications intersect at $\theta_{\mathrm{int}} = 2.91$, yielding a first-order phase transition. As expected, the temperature θ_{int} is slightly shifted to lower temperatures as compared to the MFA result.

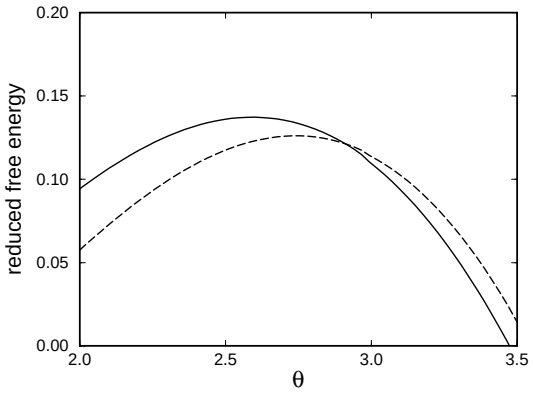

Figure 5. MFTM values for the reduced free energies F/M of the low-temperature (dashed line) and the high-temperature (solid line) modifications of the $q = \frac{1}{8}$ phase as function of the reduced temperature θ. The fixed parameters are $\lambda = 0.05$ and $j = j' = -1$. To improve the clarity, $F/M - \theta + 4$ is plotted.

In the MFTM method, some pseudo-spin interactions, though not those in the modulation direction (which should be the most important ones), are still replaced by an interaction of the pseudo-spins with a mean field. To make sure that this approximation is not responsible for the occurrence of internal phase transitions, Monte Carlo simulations were performed for phases with a short modulation length. No attempt was made to determine the global phase diagram.

Systems of sizes $L \times L \times M$ were simulated, with L ranging from 10 to 40. The number of layers, M, is given by the modulation length of the phase under investigation, e.g. $M = 6$ for the $q = \frac{1}{6}$ phase. This is done in order to avoid the development of fluctuations resulting from (meta-) stable phases with a larger modulation length. The standard one-spin-flip Metropolis algorithm is used.

Figure 6 shows the calculated specific heat as a function of the reduced temperature for the $q = \frac{1}{6}$ phase, for interactions given by $\lambda = 0.1$, $\kappa = -0.57$, and $j = j' = -0.5$ and a size of $30 \times 30 \times 6$. There are two different peaks. The peak at higher temperatures corresponds to a second-order phase transition to the disordered phase. In the present context, the narrow peak is the interesting one. It corresponds to the internal first-order phase transition. The resulting spin profiles for temperatures below and above the peak position compare favourably with the profiles obtained in MFA. In the inset showing the calculated energy, the discontinuous character of the internal phase transition is clearly visible.

4. Application to BCCD

Due to the pseudo-symmetry of half a lattice constant along $\boldsymbol{c}$, BCCD can be considered to be built up of successive layers of half-cells perpendicular to $\boldsymbol{c}$, which we label by the subscript ℓ. Applying the method described in reference [7] to BCCD, the symmetry-breaking atomic displacements occurring below the transition from the unmodulated high-temperature phase to the modulated phases are expanded in terms of a localized symmetry-adapted basis set; the respective coordinates (mode amplitudes) are projected onto two-valued pseudo-spin variables leading to symmetry-based pseudo-spin models. Every basis vector (symmetry-adapted local mode, SALM) describes a collective displacement of all of the atoms in a

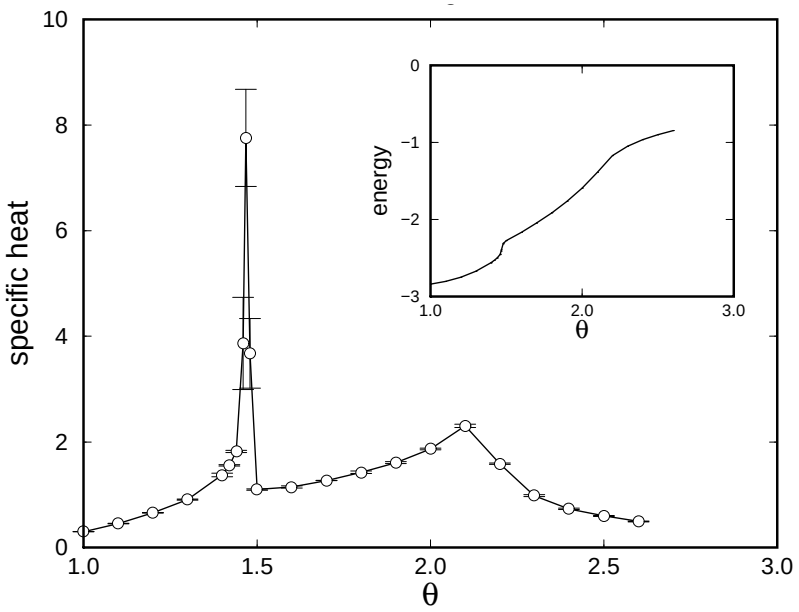

Figure 6. The specific heat of the $q = \frac{1}{6}$ phase obtained from Monte Carlo simulations of DIS systems with $30 \times 30 \times 6$ spin sites. $\lambda = 0.1$, $\kappa = -0.57$, and $j = j' = -0.5$. The inset shows the calculated energy as a function of θ.

half-cell. One obtains two relevant SALMs for the front and two for the back half-cell. Adequate superpositions of these describe structural modulations transforming according to the irreducible representations Λ_2 and Λ_3 of the group of the wave vector $\boldsymbol{q} = q\boldsymbol{c}^*$ (which is antisymmetric with respect to the mirror plane).

The pseudo-spins τ and σ represent the signs of the amplitudes of the two relevant SALMs. For convenience, we shall henceforth call the latter 'τ-SALM' and 'σ-SALM'. Previously [3, 8], we deduced the displacements corresponding to the τ- and the σ-SALMs for all BCCD atoms from experimental data [15]. For a complete visualization of these SALM displacements it is sufficient to follow the y-displacements of the nitrogen atoms. Consider the two nitrogen atoms 1 and 2 associated with a half-cell. The major parts of their y-displacements are provided by the τ-SALM contributions (equal for 1 and 2). The σ-SALM contributions (of equal sizes but opposite signs for 1 and 2) account for the small relative y-displacement of 1 and 2.

Taking the transformation properties of the SALMs into account, the form (1) of the pseudo-spin Hamiltonian is obtained as well as expressions for the spontaneous polarization in terms of the pseudo-spins [3, 8].

Experimental investigations of the pressure–temperature (p–T) phase diagram of BCCD [16–18] revealed a dielectric anomaly in the modulated phase with wave vector $\boldsymbol{k} = \frac{1}{4}\boldsymbol{c}^*$. It occurs along a line $T_S(p)$, which runs almost parallel to the boundary of the para-phase and to the lines of constant spontaneous polarization $P_{S,x}$. At ambient pressure, T_S practically coincides with the upper boundary of the fourfold phase. The T_S-anomaly exhibits the characteristics of a first-order phase transition; it leaves the wavenumber unchanged. One proposal for the explanation of the T_S-anomaly was to interpret it as a freezing of the soliton lattice [18], i.e. to assume that the soliton lattice is free to move above T_S and is pinned below.

Since the wavenumber k in BCCD is measured in units of the reciprocal lattice constant, whereas the wavenumber q in the DIS model is given in units of the reciprocal layer spacing, the $k = \frac{1}{4}$ phase in BCCD corresponds to the $q = \frac{1}{8}$ phase in the DIS formalism. For the latter the occurrence of an internal transition was explicitly demonstrated in sections 2 and 3 above. This suggests interpreting the T_S-anomaly as a manifestation of the internal transition observed in the DIS model. This hypothesis is supported by the following results.

Like the T_S-line in BCCD, the T_{int}-line runs parallel to the boundary of the high-temperature phase and parallel to the lines of constant spontaneous polarization [3]

$$P_{S,x} = \sum_{\ell}(-1)^{\ell}[P_x^1 t_\ell t_{\ell+1} + P_x^2 s_\ell s_{\ell+1} + P_x^3 s_\ell t_\ell + P_x^4(t_\ell s_{\ell+1} - s_\ell t_{\ell+1})].$$

There is an interesting connection with experimental studies on the structure of the fourfold phase in BCCD, as detailed below.

The displacement of atom μ in cell $\boldsymbol{n}$ can be written as (see, e.g., reference [19])

$$\boldsymbol{u}_{\boldsymbol{n}}^{\mu} = \sum_{m\geqslant 1}\left[\boldsymbol{e}_m^{1\mu}\cos(2\pi m\boldsymbol{k}\cdot(\boldsymbol{r}_{\boldsymbol{n}}+\boldsymbol{\rho}^{\mu})) + \boldsymbol{e}_m^{2\mu}\sin(2\pi m\boldsymbol{k}\cdot(\boldsymbol{r}_{\boldsymbol{n}}+\boldsymbol{\rho}^{\mu}))\right] \quad (11)$$

where the zeroth-order harmonics are absorbed in the average positions $\boldsymbol{\rho}^{\mu}$ of μ with respect to the origin of the cell. There are only odd harmonics due to the symmetry of the $k = \frac{1}{4}$ phase in BCCD. A comparison of the symmetries of the eigenvectors $\boldsymbol{e}_m^{1\mu}$ and $\boldsymbol{e}_m^{2\mu}$ for odd m and of the τ-SALM and the σ-SALM shows that the sine and cosine terms in (11) correspond to the t-profile and s-profile respectively [8].

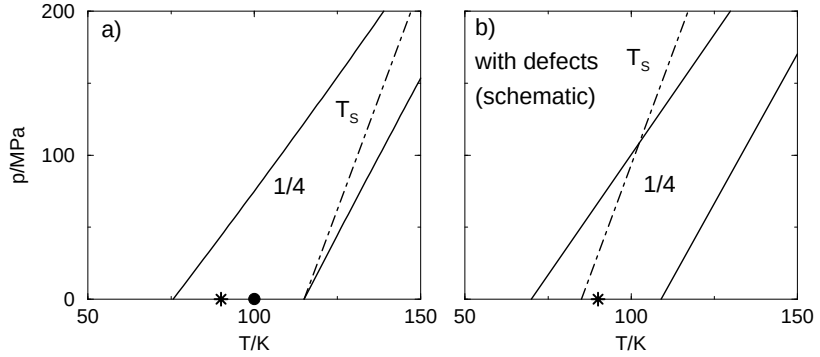

Figure 7. The p–T phase diagram of BCCD near the $k = 1/4$ phase. Solid lines: boundaries of the fourfold phase; chain lines: the T_S-anomaly. •: neutron scattering measurements [19]; ∗: x-ray diffractometry [15]. (a) The undisturbed sample (data from reference [18]). At ambient pressure, T_S coincides with the upper phase boundary. (b) The sample for which x-ray-induced defects are (schematically) taken into account. The temperature decrease is larger for T_S than for the phase boundaries. X-ray measurements at ∗ should establish the structure above T_S even at ambient pressure.

Recent neutron scattering studies [19] of the fourfold phase in BCCD at 100 K and ambient pressure (see figure 7(a), i.e. below $T_S \approx 115$ K, revealed a strong third harmonic in the cosine terms in (11). This is in perfect agreement with the structure of the low-temperature modification in the DIS model as derived in sections 2 and 3. X-ray techniques [15] showed a more sinusoidal modulation ($T = 90$ K; ambient pressure), which can be well described as the high-temperature modification in the DIS model, i.e. the one that is expected to be stable above T_S.

These seemingly contradictory experimental results can be explained if the influence of point defects on the phase diagram and recent experiments on intentionally x-ray-irradiated samples are taken into consideration. Exposure to x-rays—even to the doses used normally in diffractometry [20, 17]—produces radiation damage, which is sufficient to cause an observable lattice expansion. The effect is comparable to that of doping with bromine ions. The resulting (positive) plastic strains shift the boundaries in the p–T phase diagram to higher pressures/lower temperatures. It was observed experimentally that this shift is stronger for the T_S-line than for the other phase boundaries [17, 18]. This leads to the situation described schematically in figure 7(b): the irradiation defects induced by the x-ray measurements produce different shifts of the T_S-line and the other boundaries, and thus open up a window for the observation of the high-temperature modification of the $k = \frac{1}{4}$ phase at ambient pressure.

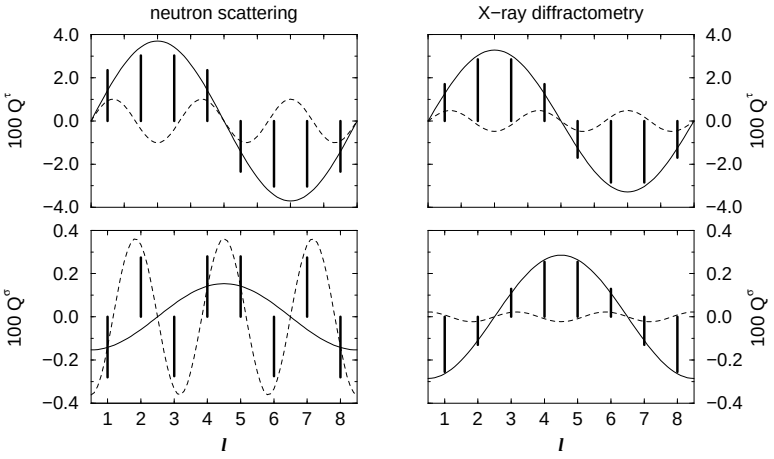

Figure 8. The fourfold phase of BCCD: the amplitudes Q_ℓ^τ and Q_ℓ^σ of the τ- and σ-SALMs as determined by the corresponding decompositions of neutron [19] (left-hand side) and x-ray [15] (right-hand side) data. In a Fourier series expansion, only first-order and third-order (solid and dashed lines respectively) harmonics in sine (cosine) are present in the spatial modulation of Q_ℓ^τ (Q_ℓ^σ). The neutron scattering results [19] show a much stronger third harmonic in the σ-SALM profile than the x-ray diffraction measurements [15].

For a more quantitative comparison of the structures predicted by the symmetry-based DIS model with the atomic displacements observed by means of either x-ray or neutron measurements, we derived the amplitudes Q_ℓ^τ and Q_ℓ^σ in a decomposition of the structural modulation in the fourfold phase of BCCD in terms of the τ- and σ-SALMs (see figure 8) from the experimental data given in references [19, 15]. In the procedure employed [3], Q_ℓ^τ and Q_ℓ^σ are proportional to t_ℓ and s_ℓ in the linear approximation. Q_ℓ^τ and Q_ℓ^σ can be written in terms of first- and third-order harmonics as in equations (4) and (5). We obtained $a_3/a_1 = 0.15$, $b_3/b_1 = -0.08$ from the x-ray data [15] and $a_3/a_1 = 0.27$, $b_3/b_1 = 2.35$ from the neutron results [19]. Similar values can be found in the DIS model for temperatures not too far above θ_{int} (e.g. $\theta = 4.25$: $a_3/a_1 = 0.18$, $b_3/b_1 = -0.07$) or below θ_{int} (e.g. $\theta = 2.76$: $a_3/a_1 = 0.39$, $b_3/b_1 = 2.13$) respectively. It is noteworthy that even with the parameters ($\lambda = 0.05$, $j = j' = -1.0$) which were rather arbitrarily chosen in this comparison and which probably do not represent the optimal choice (e.g. by the methods discussed in reference [3]) for BCCD, we find a good agreement between theoretical prediction and experimental observation.

5. Conclusions

Recent theoretical developments in the field of modulated systems allow one, in a physically well motivated way, to bridge the gap between pseudo-spin model parameters and properties on the one hand, and experimental control parameters and physical characteristics of real systems on the other.

An efficient pseudo-spin model, which is well suited as a basis both for largely analytical calculations and for numerical simulations, is the DIS model. It can be used advantageously for the theoretical description of a large class of modulated materials. Since the model variables are explicitly related to local properties of the discrete crystal lattice, it allows explicit predictions e.g. of structures, symmetries, spontaneous polarizations, phase diagrams, and orders of transitions of modulated phases in real systems, to be made.

A special feature of the DIS model is that it predicts phase transitions not only between modulated structures with different wavenumbers, but also between modulations with the same wavenumber but different pseudo-spin configurations ('internal' phase transitions). The respective phases differ significantly in the amplitudes of the harmonics in a Fourier expansion of the pseudo-spin profiles and in symmetry. Since remotely similar theoretical results derived for the ANNNI model were later shown to be artefacts of the mean-field approximation employed, we verified the validity of our MFA results by means of both the mean-field transfer-matrix method and Monte Carlo simulations.

One indication of the suitability of the symmetry-based DIS model for the description even of detailed characteristics of complex modulated real systems is the proposed explanation of the dielectric anomaly T_S observed in the fourfold phase of BCCD: this anomaly and its characteristic properties can be well interpreted as a realization of the internal phase transitions of the DIS model.

Furthermore, an application of the general procedure for translating model properties to characteristics of real, experimentally investigated systems allows a tentative explanation of the discrepancies between the experimental structure determinations of the fourfold phase of BCCD by means of neutrons on the one hand and by means of x-rays on the other. Taking the influence of x-ray-induced defects (via the strain field) into account, we propose a mechanism which allows the high-temperature modification of the fourfold phase (which exists in ideal crystals only at elevated pressure) to be already stable at ambient pressure and, thus, be apparent in x-ray measurements. The two experimentally determined structures of the fourfold phase agree fairly well with our calculated data.

Acknowledgments

Stimulating discussions with Professor Dr J M Pérez-Mato, Bilbao, and financial support from the Deutsche Forschungsgemeinschaft (research grant Si 358/2) are gratefully acknowledged.

References

[1] The status of the present experimental situation is given by
Schaack G and Le Maire M 1998 *Ferroelectrics* **208+209** 1

[2] Blinc R and Levanyuk A P (ed) 1986 *Fundamentals (Incommensurate Phases in Dielectrics 1)* (Amsterdam: North-Holland)
Selke W 1992 *Phase Transitions and Critical Phenomena* vol 15, ed C Domb and J L Lebowitz (London: Academic) p 1

[3] Neubert B, Pleimling M and Siems R 1998 *Ferroelectrics* **208+209** 141

[4] Thomas H 1971 *Structural Phase Transitions and Soft Modes* ed E J Samuelsen, E Andersen and J Feder (Oslo: Universitetsforlaget) p 15
[5] Pleimling M and Siems R 1994 *Ferroelectrics* **151** 69
[6] Pleimling M and Siems R 1996 *Ferroelectrics* **185** 103
[7] Neubert B, Pleimling M and Siems R 1998 *J. Korean Phys. Soc.* **32** S36
[8] Neubert B 1998 *Symmetriebasierte mikroskopische Modelle für modulierte Materialien* (Saarbrücken: Pirrot)
[9] Pleimling M, Neubert B and Siems R 1998 *J. Phys. A: Math. Gen.* **31** 4871
[10] Jensen M H and Bak P 1983 *Phys. Rev.* B **27** 6853
Siems R and Tentrup T 1989 *Ferroelectrics* **98** 303
[11] Selke W 1988 *Phys. Rep.* **170** 213
[12] Yokoi C S O 1991 *Phys. Rev.* B **43** 8487
Cadorin J L and Yokoi C S O 1993 *Brazilian J. Phys.* **23** 382
[13] Nakanishi K 1992 *J. Phys. Soc. Japan* **61** 2901
[14] Rotthaus F and Selke W 1993 *J. Phys. Soc. Japan* **62** 378
[15] Ezpeleta J M, Zúñiga F, Pérez-Mato J M, Paciorek W and Breczewski T 1992 *Acta Crystallogr.* B **48** 261
[16] Schaack G, Le Maire M, Schmitt-Lewen M, Illing M, Lengel A, Manger M and Straub R 1996 *Ferroelectrics* **183** 205
[17] Le Maire M 1996 Einfluß von Gitterdefekten auf die modulierten Phasen von Betain-Calciumchlorid-Dihydrat *PhD Thesis* Würzburg
[18] Le Maire M, Straub R and Schaack G 1997 *Phys. Rev.* B **56** 134
[19] Hernandez O, Quilichini M, Cousson A, Paulus W, Kiat J-M, Goukassov A, Ezpeleta J M, Zúñiga F J, Pérez-Mato J M, Dušek M and Petříček V 1998 *Proc. Aperiodic 1997* at press
Hernandez O 1997 Étude par diffusion de neutrons du chlorure de calcium et de bétaine dihydraté sous champ externe appliqué (température, champ électrique et pression hydrostatique *PhD Thesis* Paris
[20] Kiat J M, Calvarin G, Chaves M R, Almeida A, Klöpperpieper A and Albers J 1995 *Phys. Rev.* B **52** 798